Appl. Phys. B 65, 433–440 (1997)

Applied Physics B Lasers and Optics

Invited paper

Bose–Einstein condensation of lithium

C.A. Sackett, C.C. Bradley, M. Welling, R.G. Hulet

Physics Department and Rice Quantum Institute, Rice University, Houston, Texas 77005 USA

Received: 4 June 1997

Abstract. Bose–Einstein condensation of ^{7}Li has been studied in a magnetically trapped gas. Many-body quantum theory predicts that the occupation number of the condensate is limited to about 1400 atoms because of the effectively attractive interactions between ^{7}Li atoms. Using a versitile phase-contrast imaging technique, we experimentally observe the condensate number to be consistent with this limit. We discuss our measurements, the current theoretical understanding of BEC in a gas with attractive interactions, and future experiments we hope to perform.

PACS: 03.75.Fi; 05.30.Jp; 32.80.Pj

Bose–Einstein condensation (BEC) has been observed in magnetically trapped atomic gases of ^{87}Rb [1], ^{7}Li [2, 3], and ^{23}Na [4, 5]. Although the condensates are still very dilute gases, the interactions between atoms can still play a significant role in determining their physical properties. In the case of ^{7}Li, where the interactions are effectively attractive, they are thought to prevent BEC from occurring at all in a homogeneous gas [6, 7]. However, in a system with finite volume, such as a trapped gas, BEC is possible, but the number of atoms in the condensate is limited [8–17]. For ^{7}Li in our trap, the predicted limit is about 1400 atoms.

We originally reported evidence for BEC in ^{7}Li in [2]. In that work, we were not able to observe the condensate directly, so that quantitative analysis was difficult. Although we were unable to directly measure the number of condensate atoms, N_0, a simple initial analysis of the phase-space density suggested that N_0 might be as high as 10^5, which was considerably greater than expected. We have subsequently refined the analysis technique, and have shown that the original measurements were consistent with the predicted limit for N_0 [18]. Furthermore, we have now observed BEC directly, and have thus measured more precise values for N_0, again in agreement with theory [3]. In this report, we briefly describe the current theoretical understanding of BEC in a gas with attractive interactions, and then discuss our new measurements and their analysis. Finally, we describe some of the experiments we hope to perform in order to further investigate this phenomenon.

1 Theory

Interactions between ultracold bosons may be characterized by a single parameter, the s-wave scattering length a [19]. The magnitude of a indicates the strength of the interaction, while the sign determines whether the interactions are effectively attractive ($a < 0$) or repulsive ($a > 0$). The scattering length for ^{7}Li is known to be -1.45 ± 0.04 nm [20, 21]. Only two-body interactions need be considered for densities n such that $na^3 \ll 1$, which is the case for the experimentally achieved densities of $n < 10^{13}\,\mathrm{cm}^{-3}$.

The effects of attractive interactions on the condensate have been studied using mean-field theory, and neglecting inelastic collisions [8–17]. In this approximation, the interaction part of the Hamiltonian is replaced by its mean value, resulting in an interaction energy of $U = 4\pi\hbar^2 an/m$, where m is the atomic mass [19]. Because $a < 0$, U decreases with increasing n, making the gas mechanically unstable and causing the condensate to collapse upon itself. In a system with finite volume, however, the zero-point kinetic energy of the atoms provides a stabilizing influence. For a gas at zero temperature, the net result of these effects can be determined by solving the non-linear Schrödinger equation for the wave function of the condensate, $\psi(r)$ [22]:

$$\left(-\frac{\hbar^2}{2m}\nabla^2 + V(r) + U(r) - \mu\right)\psi = 0. \tag{1}$$

Here μ is the chemical potential, and $V(r)$ is the confining potential provided by the trap. In a spherically-symmetric harmonic trap with oscillation frequency ω, $V(r) = m\omega^2 r^2/2$. The interaction energy $U(r)$ is determined by taking $n(r) = N_0|\psi(r)|^2$. A numerical solution to (1) is found to exist only when N_0 is smaller than a limiting value $N_{0\,\max}$ [8]. Physically, this limit can be understood as requiring that the interaction energy U be small compared to the trap level spacing $\hbar\omega$, so that the interactions act as a small perturbation to the

ideal-gas solution. This condition implies that $N_{0\,\max}$ is of the order $l_0/|a|$, where $l_0 = (\hbar/m\omega)^{1/2}$ is the length scale of the single-particle trap ground state. It is at first surprising that $N_{0\,\max}$ increases proportional to l_0, since it is known that BEC cannot occur in a homogeneous gas. However, the density of the condensate, N_0/l_0^3, tends to zero as $l_0 \to \infty$. This tradeoff between $N_{0\,\max}$ and n is an important consideration when designing an experiment.

For condensate occupation numbers below $N_{0\,\max}$, ψ is determined using (1). It is found that for $N_0 \ll N_{0\,\max}$, ψ is closely approximated by the single-particle ground state, and as N_0 increases, the interaction energy causes the spatial extent of ψ to decrease. Note that even when a solution to (1) exists it represents only a metastable state of the trapped atoms [10, 13, 15, 16], since the equilibrium state of lithium at low temperatures is a crystalline metal solid. Also, for temperatures $T > 0$, (1) must be modified to take into account the presence of thermally excited atoms, and $N_{0\,\max}$ is slightly lower [16, 17].

Several authors, including Kagan et al. [10], Shuryak [13], and Stoof et al. [15, 16], have considered the decay of the condensate resulting from attractive two-body interactions. One of the proposed techniques is a variational method [12, 13, 15], which we discuss here following the development of Stoof. The ground-state solution to (1), ψ_0, satisfies an extremal condition

$$\langle\psi_0|H|\psi_0\rangle \le \langle\psi|H|\psi\rangle \tag{2}$$

for any other function ψ. The energy operator H is given by

$$H = -\frac{\hbar^2}{2m}\nabla^2 + V(r) + \frac{U(r)}{2}, \tag{3}$$

where the factor of $1/2$ in the interaction term arises from the dependence of U on ψ. Because the solution to (1) for the ideal gas is a Gaussian function, it is reasonable to minimize $\langle H\rangle$ using the set of Gaussian trial wavefunctions

$$\psi(r; l) = \left(\frac{N_0}{\pi^{3/2} l^3}\right)^{1/2} \exp\left(-\frac{r^2}{2l^2}\right). \tag{4}$$

Evaluating $H(l) \equiv \langle H\rangle$ yields

$$H(l) = N_0 \frac{\hbar^2}{m}\left(\frac{3}{4l^2} + \frac{3l^2}{4l_0^4} - \frac{|a|}{\sqrt{2\pi}}\frac{N_0}{l^3}\right). \tag{5}$$

This function is plotted for three values of N_0, in Fig. 1. It is observed that for sufficiently small N_0, a local minimum exists near $l = l_0$, indicating that a metastable condensate is possible. For larger N_0, however, the minimum vanishes, and the system will be unstable. The condition for metastability is $N_0 \le 0.68\, l_0/|a|$, which is in reasonable agreement with the exact value obtained by numerical integration of (1), $N_{0\,\max} = 0.58\, l_0/|a|$ [8]. At very small l, the density is sufficiently high that (1) is no longer valid, so the divergence of H as $l \to 0$ is of no concern, since it means only that the true ground state of the system is not a dilute gas.

We have extended the variational calculation to the case of a cylindrically symmetric trap with potential energy

$$V(\varrho, z) = \frac{m}{2}(\omega_\varrho^2 \varrho^2 + \omega_z z^2). \tag{6}$$

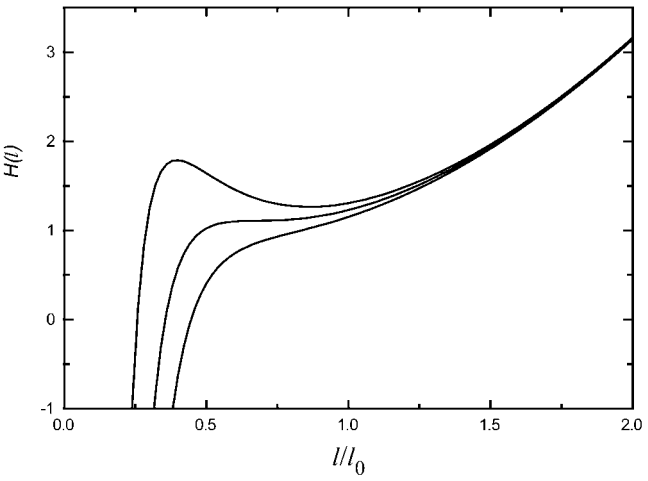

Fig. 1. The condensate energy H, plotted in units of $N_0\hbar^2/ml_0^2$. The upper curve corresponds to $N_0 = 0.48\,|a|/l_0$, the middle curve to $N_0 = 0.68\,|a|/l_0$, and the lower curve to $N_0 = 0.87\,|a|/l_0$. It is evident that a local minimum in H exists near $l = l_0$ if N_0 is sufficiently low, indicating that a metastable condensate can exist

Using a Gaussian trial wave function

$$\psi = \left(\frac{N_0}{\pi^{3/2} l_\varrho^2 l_z}\right)^{1/2} \exp\left(-\frac{\varrho^2}{2l_\varrho^2} - \frac{z^2}{2l_z^2}\right), \tag{7}$$

$\langle H\rangle$ is given by

$$H(l_\varrho, l_z) = \frac{N_0\hbar^2}{4m}\left(\frac{2}{l_\varrho^2} + \frac{1}{l_z^2} + \frac{2l_\varrho^2}{l_{0\varrho}^4} + \frac{l_z^2}{l_{0z}^4} - \frac{4}{\sqrt{2\pi}}\frac{N_0|a|}{l_\varrho^2 l_z}\right), \tag{8}$$

where $l_{0i} = (\hbar/m\omega_i)^{1/2}$. The condensate will be stable if $H(l_\varrho, l_z)$ has a local minimum. Defining $q_i = l_i/l_{0i}$ and setting $\nabla H = 0$ yields the equations

$$-\frac{1}{q_\varrho^3} + q_\varrho + \frac{\beta}{q_\varrho^3 q_z} = 0 \tag{9}$$

and

$$-\frac{1}{q_z^3} + q_z + \frac{\beta\epsilon^2}{q_\varrho^2 q_z^2} = 0, \tag{10}$$

where $\beta = (2/\pi)^{1/2} N_0|a|/l_{0z}$ is proportional to the strength of the interactions, and $\epsilon = l_{0z}/l_{0\varrho}$ is the asymmetry of the trap. Eliminating q_ϱ yields the single condition

$$f(q_z) \equiv q_z^4 + \beta\epsilon^2 \frac{q_z^{3/2}}{\sqrt{q_z - \beta}} - 1 = 0. \tag{11}$$

Since f diverges to $+\infty$ on either end of its range, solutions to (11) will exist if and only if the minimum value of f is less than or equal to zero. The critical value of β is therefore found by requiring the minimum value of f to be zero, which occurs when $f = 0$ and $f' = 0$ at the same value of q_z. These equations can be solved numerically, or analytical expressions can be found in the limits of large and small ϵ. For $\epsilon \gg 1$, the roots of f occur at small q_z, so that the q_z^4 term

can be neglected. The stability condition is then $\beta < 0.62/\epsilon$, or $N_{0\ \max} \approx 0.78\, l_{0\varrho}/|a|$. For $\epsilon \ll 1$, (11) can be expanded around $q_z = 1$ and $\beta = 1$. The critical value of β is found to be $1 - 0.75\,\epsilon^{4/3}$, giving $N_{0\ \max} \approx 1.25\, l_{0z}/|a|$. In both limits, the stability condition can be expressed as

$$N_{0\ \max} \approx \frac{l_{min}}{|a|}, \tag{12}$$

where l_{min} is the lesser of $l_{0\varrho}$ and l_{0z}. This result indicates that a spherically symmetric trap is optimal for most purposes, as it provides the highest density for a given $N_{0\ \max}$.

The variational model also allows exploration of the dynamics of the condensate, if l is interpreted as the coordinate of a quasiparticle moving in the potential $H(l)$. The energy levels of the quasiparticle potential then correspond to excitations of the "breathing mode" of the condensate. In particular, Stoof has calculated decay rates for the metastable state due both to thermal fluctuations and to quantum mechanical tunneling through the barrier [15]. The decay rate is found to be negligible until N_0 is within a few hundred atoms of $N_{0\ \max}$, for conditions comparable to our experiments. Because of the limited class of wave functions considered in (4), Stoof's result is only applicable to decays which take place via the breathing mode, in which the entire condensate collapses at once. Under our conditions, this decay mode is expected to dominate, as it is the only mode found whose excitation frequency approaches zero as $N_0 \to N_{0\ \max}$ [12]. However, another approach has been used to investigate decay channels in which only a fraction of the condensate participates in the collapse, by estimating the overlap between the metastable state and various denser collapsing states [10, 13]. Although both of these methods provide useful insight, a comprehensive theory of the collapse has not yet been developed.

The dynamics of the collapse itself are also interesting, but a detailed theoretical description is challenging, because the density can become large enough that many-body interactions must be considered. However, while the density remains low, the evolution of the condensate can be described by the motion of the quasiparticle in the potential H. By calculating this trajectory and including losses due to inelastic collisions, Stoof has found that essentially all the collapsing atoms are ejected from the trap before the density rises so high that the dilute-gas approximation becomes invalid [23]. For a trapped gas at $T > 0$, only those atoms not initially in the condensate will remain after the collapse, so the gas will be in a non-equilibrium distribution. Elastic collisions rethermalize the gas, and N_0 will grow again. If the gas is actively cooled, then the condensate will continue to fill and collapse until either $T = 0$ is reached or no atoms remain. We have modeled the population dynamics of this system using the quantum Boltzmann equation, and show a typical result for $N_0(t)$ in Fig. 2. These calculations will all be elaborated upon in a future publication.

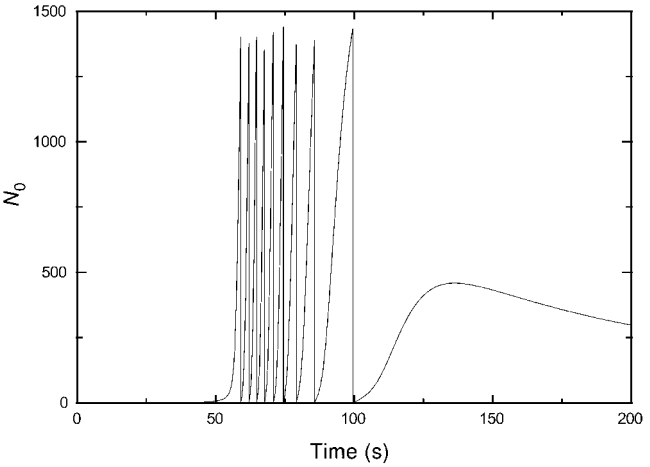

Fig. 2. Evolution of the number of condensate atoms during evaporative cooling. At early times, corresponding to high temperatures, the number of condensate atoms is negligible, but as the gas is cooled to the critical point, N_0 begins to rise. When N_0 approaches the stability limit $N_{0\ \max}$, the rates for thermal and quantum mechanical fluctuations increase, until eventually the condensate collapses. It is expected that the entire condensate collapses at once, effectively reducing N_0 to zero. Elastic collisions then repopulate the condensate, and the cycle continues until too few atoms remain to cause a collapse. The remaining atoms are then gradually lost through inelastic collisions

2 Experiment

The apparatus used to produce BEC has been discussed in detail in previous publications [2, 3, 24]. The magnetic trap is an Ioffe design, constructed from six cylindrical permanent magnets. The atoms are trapped in the doubly spin polarized ground state, where they experience a nearly symmetric harmonic potential with oscillation frequencies $\nu_x = 150.6$ Hz, $\nu_y = 152.6$ Hz, and $\nu_z = 131.5$ Hz. The magnetic field at the center of the trap is directed along the z-axis, with a magnitude of 1003 G. This field configuration prevents losses due to nonadiabatic spin-flip transitions which can occur near a field zero [25–27]. The trap is loaded from a laser-slowed atomic beam, and the dissipation needed to capture the atoms is provided by six laser beams tuned near the $2S_{1/2}$ ($F = 2$, $m_F = 2$) $\leftrightarrow$ $2P_{3/2}$ ($F = 3$, $m_F = 3$) cycling transition. The number of trapped atoms N reaches a maximum of approximately 2×10^8, after a few seconds of loading. These atoms are precooled to about 200 μK by Doppler laser cooling, and have a peak density of roughly 1×10^{11} cm^3.

After switching off the laser beams, the atoms are further cooled by forced evaporative cooling [28]. The hottest atoms are driven to an untrapped ground state by a microwave field tuned just above the ($F = 2$, $m_F = 2$) $\leftrightarrow$ ($F = 1$, $m_F = 1$) Zeeman transition frequency of approximately 3450 MHz. As the atoms cool, the microwave frequency is reduced. The frequency vs. time trajectory that maximizes the phase-space density of the trapped atoms is calculated ahead of time [29], and depends on the elastic collision rate and the trap loss rate. The elastic collision rate $n\sigma v$ is roughly $1\,\mathrm{s}^{-1}$, with cross-section $\sigma = 8\pi a^2 \approx 5 \times 10^{-13}$ cm^2. The elastic collision rate is approximately constant during evaporative cooling. The loss rate due to collisions with hot background gas atoms is $1.6 \times 10^{-3}\,\mathrm{s}^{-1}$, and inelastic dipolar-relaxation collisions occur with a rate constant of 10^{-14} cm^3/s [30]. Quantum degeneracy is typically reached after roughly 200 seconds, with $N \approx 10^5$ atoms at $T \approx 300$ nK, although fluctuations in the loading conditions produce some variation in the results of evaporative cooling. Lower temperatures are reached by extending the cooling time.

After evaporative cooling, the rf field is removed, and the atoms are allowed to equilibrate for a few seconds. The

spatial distribution of atoms is then imaged in situ using an optical probe. The single-particle harmonic oscillator ground state of our trap has a Gaussian density distribution with a 1/e-radius of 3 μm. The resolution of the imaging system must therefore be sufficient to detect such a small object. In our original experiment [2], the imaging resolution was not sufficient, but the presence of the condensate was deduced from distortions observed in images of quantum degenerate clouds. We have since developed a comprehensive model of these distortions, which is explained in detail in [18]. In that work, we find that the presence of a condensate should cause such distortions, given the imaging system that was used.

We have subsequently improved our imaging, and now use a system shown schematically in Fig. 3. With the polarizer E removed, it can be used to measure the density distribution by absorption imaging, in which the absorptive shadow of the atoms is imaged onto the camera. However, the atom cloud causes both an attenuation and a phase shift of the probe laser beam. Near resonance, the phase shift can be large, and any imaging system with finite resolution will be sensitive to this phase to some extent. This sensitivity can cause significant image distortions, which are readily detected through their dependence on the probe detuning Δ. In order to eliminate such distortions, it is necessary to reduce the index of refraction by using large Δ. However, since the absorption coefficient decreases as Δ^{-2}, while the phase shift decreases as only Δ^{-1}, eliminating the distortions can leave the absorption signal too small to be detected.

This problem can be solved by using phase-contrast imaging, a common technique in microscopy [31]. The net effect of the atoms on the incident electric field $\boldsymbol{E}_0$ can be described by a complex phase β, such that immediately after the cloud the field is $\boldsymbol{E} = \boldsymbol{E}_0 \mathrm{e}^{\mathrm{i}\beta}$. The phase $\beta(r)$ depends on position, and has real and imaginary parts given by $\beta = \phi + \mathrm{i}\alpha/2$, where ϕ is the dispersive phase shift and α is the optical density of the cloud. In absorption imaging, the detected signal intensity I_s depends only on α: $I_\mathrm{s} = I_0|\mathrm{e}^{\mathrm{i}\beta}|^2 = I_0\mathrm{e}^{-\alpha}$, where $I_0 = |\boldsymbol{E}_0|^2$. Phase-contrast techniques consist of controlled ways to produce an image intensity which depends on ϕ. In the simplest technique, dark-field imaging, a spatially small opaque beam block is inserted at a focus of the probe laser beam (position D in Fig. 3), thus blocking the probe beam and passing all but a negligible amount of the scattered light. The resulting signal is $I_\mathrm{s} = I_0|\mathrm{e}^{\mathrm{i}\beta} - 1|^2 \approx I_0\phi^2$ for $\alpha \ll |\phi| \ll 1$. Andrews et al. used this technique to image ^{23}Na Bose–Einstein condensates in situ [32]. However, in order to minimize refractive distortions it is desirable that $|\phi| \ll 1$, so the dark-field signal becomes relatively small as it is proportional to ϕ^2.

A more sensitive method for phase-contrast imaging, in which the signal depends linearly on ϕ, exploits the birefringence of the atoms in a strong magnetic field [3]. The probe beam propagates in the (1, 1, 1) direction of a coordinate system in which the z-axis is parallel to the bias field, and the x- and y-axes are the symmetry axes of the quadrupole field. The probe is linearly polarized with polarization vector $\hat{\epsilon}_0 = (1, -1, 0)/\sqrt{2}$. The electric field therefore decomposes into two elliptical polarizations $\boldsymbol{E} = \boldsymbol{E}_\mathrm{c} + \boldsymbol{E}_\mathrm{nc}$, such that $\boldsymbol{E}_\mathrm{c}$ couples to the σ^+ cycling transition and acquires the phase shift $\exp(\mathrm{i}\beta)$, while $\boldsymbol{E}_\mathrm{nc}$ does not. The polarization vector of $\boldsymbol{E}_\mathrm{c}$ is $\hat{\epsilon}_c = (3+\mathrm{i}, -3+\mathrm{i}, -2\mathrm{i})/\sqrt{24}$, and the uncoupled polarization is $\hat{\epsilon}_{nc} = (1+\mathrm{i}, 1-\mathrm{i}, -2)/\sqrt{8}$, so after passing through the atoms, the field can be expressed as

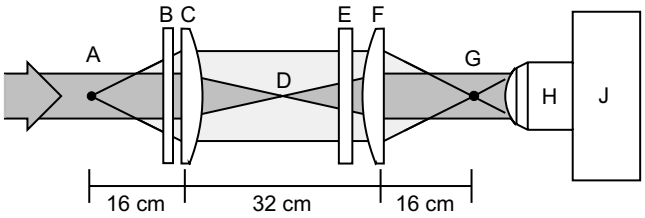

Fig. 3. A schematic of the imaging system used for in situ phase-contrast polarization imaging. A linearly polarized laser beam is directed through the cloud of trapped atoms located at A. The probe beam and scattered light field pass out of a vacuum viewport B, and are relayed to the primary image plane G by an identical pair of 3-cm-diameter, 16-cm-focal-length doublet lenses C and F. The light is then re-imaged and magnified onto a camera J by a microscope objective H. The measured magnification is 19, and the camera pixels are 19 μm square. A linear polarizer E can be used to cause the scattered light and probe fields to interfere, producing an image sensitive to the refractive index of the cloud. The system is focussed by adjusting the position of lens F, which is mounted on a translator. Reprinted from [3] by permission

$$\boldsymbol{E} = E_\mathrm{c}\mathrm{e}^{\mathrm{i}\beta}\hat{\epsilon}_\mathrm{c} + E_\mathrm{nc}\hat{\epsilon}_\mathrm{nc}. \tag{13}$$

By passing the light through a polarizer (E in Fig. 3), the components $\boldsymbol{E}_\mathrm{c}$ and $\boldsymbol{E}_\mathrm{nc}$ can be coherently recombined. For a polarizer transmitting light with polarization $\hat{n}$, the signal detected on the camera, $|\hat{n}\cdot\boldsymbol{E}|^2$, is a phase-contrast image of the cloud. A straightforward calculation gives the detected signal

$$\begin{aligned} I_\mathrm{s} = \frac{I_0}{16}\Big[&\cos^2\theta\left(1 + 9\mathrm{e}^{-\alpha} + 6\mathrm{e}^{-\alpha/2}\cos\phi\right) \\ &+ \sin^2\theta\left(3 + 3\mathrm{e}^{-\alpha} - 6\mathrm{e}^{-\alpha/2}\cos\phi\right) \\ &- 8\sqrt{3}\sin\theta\cos\theta\mathrm{e}^{-\alpha/2}\sin\phi\Big], \end{aligned} \tag{14}$$

where θ is the angle between $\hat{n}$ and $\hat{\epsilon}_0$. Usually, the probe detuning is large enough that ϕ is small and α can be neglected, so that the signal can be expanded as

$$I_\mathrm{s}(r) = I_0(\cos^2\theta + \frac{\sqrt{3}}{4}\phi(r)\sin 2\theta - \frac{3}{16}\phi(r)^2\cos 2\theta), \tag{15}$$

Linear phase-contrast imaging is accomplished for $\theta = 45°$ and dark-field imaging is recovered for $\theta = 90°$. By varying θ between these extremes, the relative size of the signal and background can be varied in order to maximize the signal-to-noise ratio of the image. For the data reported here, $\theta = \pm 75°$.

The probe beam is pulsed on for a duration of 10 μs, at an intensity of 250 mW/cm^2 and with Δ in the range $20\Gamma < |\Delta| < 40\Gamma$, where $\Gamma = 5.9$ MHz is the natural linewidth of the transition. Only one image can be obtained under these conditions, because each atom scatters a few photons while being probed, heating the gas to several μK.

The detected signal intensity, given by (15), is proportional to the column density of the trapped atoms, since [33]

$$\beta(x', y') = \phi + \mathrm{i}\frac{\alpha}{2} = -\frac{\sigma_0}{2}\int dz'\, n(x', y', z')\,\frac{\Gamma}{2\Delta + \mathrm{i}\Gamma}, \tag{16}$$

where $\sigma_0 = 1.43\times10^{-9}\,\mathrm{cm}^2$ is the resonant light scattering cross section λ^2/π. The z'-axis is parallel to the probe propagation axis, and the x'- and y'-axes lie in the image plane.

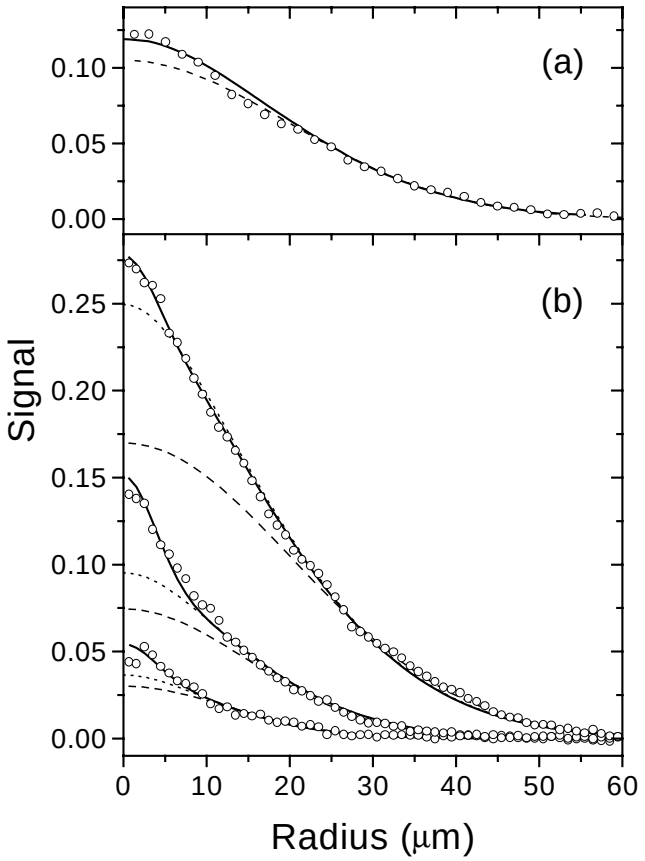

Fig. 4a,b. Spatial image profiles of trapped ultracold ^{7}Li gas. The vertical axis gives the magnitude of the phase-contrast signal intensity relative to the probe intensity, which is proportional to the column density of the gas. The data points are taken from observed images. The solid curves are calculated by fitting Bose-Einstein distributions to the data, the short-dashed curves are the same distributions with the condensate atoms removed, and the long-dashed curves are classical (Gaussian) distributions fit to the tails of the data. The calculated signals are convolved with a Gaussian function to account for the limited resolution of the imaging system, assuming an effective resolution of 4 μm. For the data in (**a**), the probe detuning was +191 MHz, and the fitted distribution has 9.0×10^4 atoms at a temperature of 309 nK. The number of condensate atoms is ~ 1, indicating that the gas is just approaching degeneracy. In (**b**) a sequence of profiles that exhibit condensate peaks are shown. From the strongest to weakest signals, the total number of atoms and fitted temperatures are: 1.01×10^5 atoms at 304 nK; 2.6×10^4 atoms at 193 nK; and 6.6×10^3 atoms at 122 nK. The corresponding numbers of condensate atoms are 500, 810, and 270, respectively. The probe laser detuning for these data was −130 MHz. Reprinted from [3] by permission

Light scattering might be modified by the quantum degenerate nature of the atoms, but this effect is expected to be negligible under our conditions [34]. Equation (16) also assumes that the atom cloud is thin enough that the laser field is not diffracted or refracted appreciably while passing through. This approximation is accurate for sufficiently small ϕ.

Because the trap is not isotropic, the density distributions are slightly ellipsoidal; the images are observed to have the expected aspect ratio of 1.10, accounting for the trap asymmetry and the oblique viewing angle. This aspect ratio will be reduced for a degenerate gas, and is 1.05 for the condensate itself. However, this difference is not discernible with our imaging resolution. Figure 4 shows radial signal profiles, which are obtained from the images by angle-averaging the data around appropriate ellipses. The various curves are the results of our analysis, which will be described in the following section.

3 Image analysis

We assume that the gas is in thermal equilibrium, and fit T and N_0 to the data. Any two of N, T, or N_0 completely determine the density of the gas through the Bose–Einstein distribution function. Given T and N_0, the density is calculated using a semi-classical ideal-gas approximation for the non-condensed atoms [35], and a Gaussian function for the condensate:

$$n(\boldsymbol{r}) = \frac{1}{\Lambda^3} \sum_{s=1}^{\infty} \frac{\zeta^s}{s^{3/2}} \exp\left[-\frac{sV(\boldsymbol{r})}{k_{\mathrm{B}}T}\right] + \frac{N_0}{\pi^{3/2} l_{0x} l_{0y} l_{0z}} \exp\left[-\left(\frac{x^2}{l_{0x}^2} + \frac{y^2}{l_{0y}^2} + \frac{z^2}{l_{0z}^2}\right)\right]. \tag{17}$$

Here $\Lambda = (2\pi\hbar^2/mk_{\mathrm{B}}T)^{1/2}$ is the thermal deBroglie wavelength, $\zeta = N_0/(N_0+1)$ is the fugacity, $V(\boldsymbol{r})$ is the trap potential $m(\omega_x^2 x^2 + \omega_y^2 y^2 + \omega_z^2 z^2)/2$, and $l_{0i} = (\hbar/m\omega_i)^{1/2}$ is the length scale of the condensate for the i-axis. The semi-classical distribution was compared to an exact calculation, and found to be accurate, except for a temperature shift as noted in [36]. All the temperatures reported here are calculated in the semi-classical approximation. The results of the fits are shown by the solid lines in Fig. 4.

For temperatures sufficiently greater than the critical temperature, the gas can be described by the Boltzmann distribution, which predicts a Gaussian density profile

$$n_B(\boldsymbol{r}) = \frac{N_0}{\Lambda^3} \exp\left[-\frac{V(\boldsymbol{r})}{k_{\mathrm{B}}T}\right], \tag{18}$$

where $N_0 = \omega_x\omega_y\omega_z(\hbar/k_{\mathrm{B}}T)^3$ in the classical limit. The long-dashed lines in Fig. 4 are Gaussian functions fit to the tails of the distributions, which approximate the data only in Fig. 4a, where the fit to the Bose–Einstein distribution indicates a near-degenerate condition, with $N_0 \approx 1$. Figure 4b shows three distributions for which $N_0 \gg 1$. For these distributions, the density is distinctly non-Gaussian, due to an enhanced central peak. Comparison between Fig. 4a and the upper curve in Fig. 4b is striking, as these distributions correspond to nearly the same temperature, and only differ by about 10% in number. From this comparison, it is clear that the gas has reached the degenerate regime, where Boltzmann statistics are inadequate. In order to illustrate the fraction of the signal due to the condensate, the theoretical contribution of the condensate was subtracted from the solid curves. The remaining signal is shown by the short-dashed curves in Fig. 4b. As comparison of the short-dashed, long-dashed and solid curves indicates, the observed increase in the peak signal is caused by both condensed and non-condensed atoms. The contribution of the non-condensed atoms is significant for the upper curve, but at lower temperatures, the contribution of the condensate makes up most of the enhanced peak.

The analysis used to obtain the above results is complicated by the fact that the condensate size is on the order of the imaging resolution. The finite resolution is included in

the fitting procedure by convolving the theoretical signal with the point-transfer function of the imaging system, $G(r)$. The point-transfer function gives the field produced at image position r by a point source at the center of the trap, and can be calculated by standard techniques [18, 37]. It depends on both the aperture size and the lens aberrations of the imaging system.

In order to test the calculation of G, we imaged laser light emerging from an optical fiber. The intensity distribution of the light in the fiber is Gaussian with a 1/e-radius of 1.2 μm, so that it approximates a point source. Figure 5 shows cross-sections of the images obtained with the system focussed at two different points. The narrower peak shown has a 1/e-radius of 3.0 μm, as compared with 2.5 μm expected for a diffraction-limited lens (dotted line). In the experiment, the focal position of the imaging system could be determined to ±200 μm, by observing distortions in images of the atom cloud which occur when the system is further off focus. The two solid curves in the figure show the variation of G across this range.

Although the convolution of the image electric field $E_0 e^{i\beta}$ with $G(r)$ is easily described, it is computationally slow to apply to a two-dimensional image. A simpler method allowing greater physical insight is to approximate $G(r)$ by a Gaussian function with 1/e-radius R. The approximation is accurate for small r, but G has a relatively large tail for large r which falls to zero more slowly than a Gaussian. However, the phase of G varies rapidly for large r, and this variation reduces the importance of the tail in the convolution integral. Convolution with a Gaussian function rather than G therefore introduces only a small error. We determined the effect of this error on the fit by comparing the values of N_0 obtained with the exact and approximate convolutions. The error in N_0 was small, and could be corrected by adjusting R to give the correct value of N_0. This procedure was carried out for various focal positions in the range of the experimental uncertainty. The values for R obtained ranged from 2.5 μm to 5.0 μm. This uncertainty is the dominant source of error in our determination of N_0.

Using the fitting procedure described above, we have found degenerate conditions for T between 120 and 330 nK, and for N between 6800 and 135 000 atoms. In all cases, N_0 is found to be relatively small. Fitting with $R = 5$ μm, the maximum N_0 observed is about 1300 atoms. Taking instead $R = 4$ μm or 2.5 μm yields a maximum N_0 of 1000 or 650 atoms, respectively. No systematic effects were observed as either the sign or the magnitude of the detuning or the polarizer angle were varied, indicating the absence of phase-dependent distortions and confirming the relations given in Eqs. (15) and (16).

In the analysis so far we have assumed that the gas is ideal, but interactions are expected to alter the size and shape of the density distribution. Mean-field theory predicts that interactions will reduce the 1/e-radius of the condensate from 3 μm for low occupation number to ∼ 2 μm as the maximum N_0 is approached [11, 14–17]. If the smaller condensate radius is assumed in the analysis, the maximum observed value for N_0 decreases, becoming ∼ 1050 for $R = 5$ μm. The size of the condensate is not expected to change appreciably for $N_0 < 1000$, so the values obtained for $R = 2.5$ μm and 4 μm are not sensitive to interactions. Effects of the interactions on the distribution of the non-condensed atoms are not expected to be significant [16, 38], because at the critical density the mean interaction energy of ∼ 1 nK is much smaller than T.

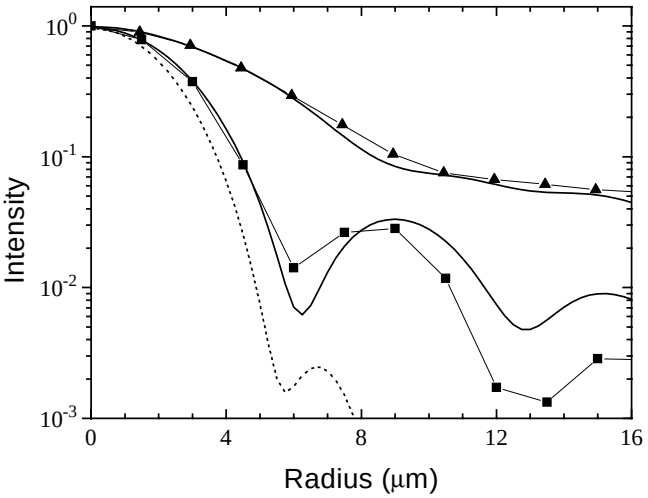

Fig. 5. Test images of an optical fiber. The data points are obtained from cross-sections through images of the light emitted by an optical fiber. The squares indicate data obtained with the imaging system at its best focus, and the triangles indicate data obtained with the system defocussed by 200 μm. The solid curves are the expected intensity patterns, and the dashed curve is the calculated pattern for a well-focussed system in the absence of lens aberrations. The calculated curves are obtained by convolving the point transfer function of the imaging system with a Gaussian electric field with 1.75 μm 1/e-radius to account for the size of the optical fiber mode, and squaring the result to obtain the intensity. The signal is then averaged to reflect the pixel size of the camera. Reprinted from [3] by permission

An estimate of our experimental sensitivity to the presence of condensate atoms can be obtained from the fitting procedure. By fixing N_0 and fitting T to the data, best-fit distributions are obtained as a function of N_0. Since N_0 mostly affects the central part of the distribution, the sensitivity to N_0 is best illustrated by considering a restricted χ_0^2 which is the sum over the squares of the differences between the calculated distributions and the data for radii less than 10 μm. Calculating $\chi_0^2(N_0)$ for several images with large values of N_0 indicates that χ_0^2 is increased by a factor of 2 from its minimum value when N_0 is varied by about 150 atoms, roughly independent of R. An example showing this variation is given in Fig. 6.

4 Conclusions and future experiments

The measurements described above have demonstrated that BEC can occur in a gas with $a < 0$. The results of our analysis indicate a number of condensate atoms which is consistent with the limit predicted by mean-field theory. However, there remain several important questions which can be addressed experimentally.

One such experiment is to determine $N_{0\,\max}$ more precisely, in order to more strictly test the quantitative predictions of mean-field theory. As previously stated, the dominant uncertainty in our determination of N_0 is the sensitivity to the effective resolution R. This sensitivity could be reduced by observing a distribution consisting mainly of condensate atoms. Because the integrated intensity of an image is independent of lens aberrations, N_0 could be measured by simply integrating the signal to determine the number of trapped

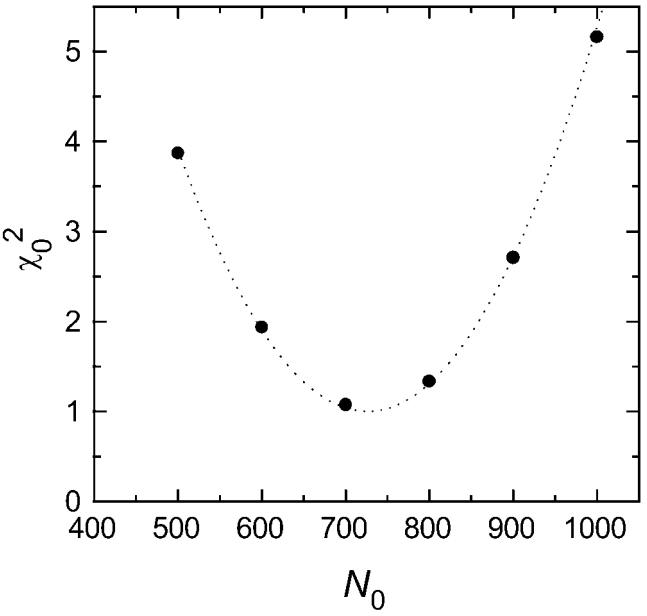

Fig. 6. Experimental sensitivity to the presence of condensate atoms. For a particular image signal profile, various values of N_0 are chosen, and for each N_0 the temperature T is adjusted to fit a Bose–Einstein distribution to the entire data set. However, only the central region of the distribution depends strongly on N_0, so χ_0^2 is defined by summing over the squares of the differences between the fit and the data for $r < 10\,\mu$m. The figure shows the resulting $\chi_0^2(N_0)$ for the data set corresponding to $N_0 = 810$ atoms shown in Fig. 4b. The effective resolution used is $R = 4\,\mu$m. The minimum value of $\chi_0^2(N_0)$ is normalized to 1. An estimate for the uncertainty in N_0 is the range across which χ_0^2 doubles, ± 125 atoms in this case. The minimum in the above curve is not located at the same value of N_0 as was obtained from the fit in Fig. 4, reflecting the fact that in the actual analysis, both T and N_0 were chosen to minimize the unrestricted χ^2, using all data points. This difference serves as an additional, and consistent, estimate of the uncertainty in N_0

atoms. It may be possible to produce such a bare condensate using evaporative cooling, but doing so is technically challenging. Among other difficulties, the trap bias field must have a relative stability of 10^{-7} so that variations in the spin-flip transition frequency are less than the trap energy-level splitting.

Another area offering exciting prospects is the study of the collapse itself. The collapse/fill model described in Sect. 1 predicts that the values of N_0 should fluctuate between zero and the limiting value during evaporative cooling, but this model has not yet been confirmed. We have observed fluctuations in N_0, but it is not clear whether they are intrinsic or whether they are caused by variations in trap loading and evaporative cooling. If these variations can be controlled and N_0 measured precisely, then measurement of the fluctuations should provide detailed information on the dynamics of the collapse and growth of the condensate.

To further probe the nature of the collapse, it may be possible to modify the scattering length by applying a laser beam tuned near a molecular resonance of Li_2 [39, 40]. However, changing a with light also introduces losses due to spontaneously scattered photons from both the molecular and the free atomic transitions. By using relatively deep-lying molecular levels, it is feasible to produce significant changes in a while maintaining a trap loss rate which is small compared to both the trap oscillation frequency ω and the mean-field interaction frequency $U/\hbar$. Unfortunately, the loss rate cannot be made small compared to the elastic collision rate, so it is not possible to produce a positive value of a and then populate the condensate using evaporative cooling. It is possible, however, to make a more negative, and thereby induce a collapse. By initiating a collapse at a definite time, this technique could allow direct investigation of the dynamics of the collapse.

Other experiments of interest include determination of the excitation spectrum, observation of soliton-like excitations and production of vortex states. We believe that, through experiments such as these, studies of condensates with $a < 0$ will provide important insights into many-body quantum theory.

Acknowledgements. We are grateful to H. Stoof for many stimulating discussions. This work is supported by the National Science Foundation, the Welch Foundation, the Texas Advanced Technology Program, and NASA. M.W. acknowledges support by the Deutsche Forschungsgemeinschaft.

References

1. M.H. Anderson, J.R. Ensher, M.R. Matthews, C.E. Wieman, E.A. Cornell: Science **269**, 198 (1995)
2. C.C. Bradley, C.A. Sackett, J.J. Tollett, R.G. Hulet: Phys. Rev. Lett. **75**, 1687 (1995)
3. C.C. Bradley, C.A. Sackett, R.G. Hulet: Phys. Rev. Lett. **78**, 985 (1997)
4. K.B. Davis, M.-O. Mewes, M.R. Andrews, N.J. van Druten, D.S. Durfee, D.M. Kurn, W. Ketterle: Phys. Rev. Lett. **75**, 3969 (1995)
5. M.-O. Mewes, M.R. Andrews, N. J. van Druten, D.M. Kurn, D.S. Durfee, W. Ketterle: Phys. Rev. Lett. **77**, 416 (1996)
6. L.D. Landau, E.M. Lifshitz: *Statistical Physics*, 1st ed. (Pergamon, London 1958)
7. H.T.C. Stoof: Phys. Rev. A **49**, 3824 (1994)
8. P.A. Ruprecht, M.J. Holland, K. Burnett, M. Edwards: Phys. Rev. A **51**, 4704 (1995)
9. G. Baym, C.J. Pethick: Phys. Rev. Lett. **76**, 6 (1996)
10. Y. Kagan, G.V. Shlyapnikov, J.T.M. Walraven: Phys. Rev. Lett. **76**, 2670 (1996)
11. F. Dalfovo, S. Stringari: Phys. Rev. A **53**, 2477 (1996)
12. K. Singh, D. Rokhsar: Phys. Rev. Lett. **77**, 1667 (1996)
13. E. Shuryak: Phys. Rev. A **54**, 3151 (1996)
14. R.J. Dodd, M. Edwards, C.J. Williams, C.W. Clark, M.J. Holland, P.A. Ruprecht, K. Burnett: Phys. Rev. A **54**, 661 (1996)
15. H.T.C. Stoof: J. Stat. Phys. **87**, 1353 (1997)
16. M. Houbiers, H.T.C. Stoof: Phys. Rev. A **54**, 5055 (1996)
17. T. Bergeman: Phys. Rev. A **55**, 3658 (1997)
18. C.C. Bradley, C.A. Sackett, R.G. Hulet: Phys. Rev. A **55**, 3951 (1997)
19. K. Huang: *Statistical Mechanics*, 2 ed. (John Wiley & Sons, New York 1987)
20. E.R.I. Abraham, W.I. McAlexander, C.A. Sackett, R.G. Hulet: Phys. Rev. Lett. **74**, 1315 (1995)
21. A.J. Moerdijk, W.C. Stwalley, R.G. Hulet, B.J. Verhaar: Phys. Rev. Lett. **72**, 40 (1994)
22. E.M. Lifshitz, L.P. Pitaevskii: *Statistical Physics, Part 2* (Butterworth-Heineman, Oxford 1980)
23. H.T.C. Stoof, private communication
24. J.J. Tollett, C.C. Bradley, C.A. Sackett, R.G. Hulet: Phys. Rev. A **51**, R22 (1995)
25. A.L. Migdall, J.V. Prodan, W.D. Phillips, T.H. Bergeman, H.J. Metcalf: Phys. Rev. Lett. **54**, 2596 (1985)
26. W. Petrich, M.H. Anderson, R.J. Ensher, E.A. Cornell: Phys. Rev. Lett. **74**, 3352 (1995)
27. K.B. Davis, M.-O. Mewes, M.A. Joffe, M.R. Andrews, W. Ketterle: Phys. Rev. Lett. **74**, 5202 (1995)
28. W. Ketterle, N.J. van Druten, in *Advances in Atomic, Molecular, and Optical Physics* (Academic Press, San Diego 1996), No. 37, p. 181
29. C.A. Sackett, C.C. Bradley, R.G. Hulet: Phys. Rev. A **55**, 3797 (1997)
30. A.J. Moerdijk, B.J. Verhaar: Phys. Rev. A **53**, R19 (1996)
31. E. Hecht: *Optics*, 2nd ed. (Addison-Wesley, Reading, MA 1987)

32. M.R. Andrews, M.-O. Mewes, N.J. van Druten, D.S. Durfee, D.M. Kurn, W. Ketterle: Science **273**, 84 (1996)
33. P. Meystre, M.S. III: *Elements of Quantum Optics*, 2 ed. (Springer, Berlin 1991)
34. O. Morice, Y. Castin, J. Dalibard: Phys. Rev. A **51**, 3896 (1995)
35. V. Bagnato, D.E. Pritchard, D. Kleppner: Phys. Rev. A **35**, 4354 (1987)
36. W. Ketterle, N.J. van Druten: Phys. Rev. A **54**, 656 (1996)
37. M. Born, E. Wolf: *Principles of Optics* (Pergamon Press, New York 1959)
38. T. Bergeman, personal communication
39. P.O. Fedichev, Y. Kagan, G.V. Shlyapnikov, J.T.M. Walraven: Phys. Rev. Lett. **77**, 2913 (1996)
40. J.L. Bohn, P.S. Julienne, to be published